3.4 Neutron–Proton Phase Shifts between 500 and 1090 MeV

Abstract. Phase-shift analyses of neutron-proton scattering were performed in the laboratory-energy range from 500 to 1090 MeV with the $I = 1$ phases being fixed to our previously determined values. A narrow resonance in the $^1P_1$ wave is not found in the solutions of single-energy analyses of the overall data, but it is detected in the solution of energy dependent analysis in the range from 500 – 800 MeV. The obtained $I = 0$ inelastic cross section in the solutions of the phase-shift analyses is consistent with our evaluated values by means of the isospin invariance.
(Prog. Theor. Phys. **95** (1996), 577.)

3.4.1 Introduction

In the last decade, a considerable amount of p-p and n-p data has been obtained in the intermediate energy region. The phase-shift analysis(PSA) of p-p scattering in this region has provided excellent results and indicated the possible existence of resonance-like structures for the isospin $I = 1$ partial waves of $^1D_2$ and $^3F_3$[9, 10, 11, 42, 59, 66, 90, 91]. The n-p data are not sufficient for a PSA-solution, relative to the p-p data.

Bystricky et al.[11] performed an energy dependent PSA of n-p scattering among the incident laboratory energies $T_L = 10 - 800$ MeV, with the data base compensated by the reconstructed inelastic total cross section[92], the energy dependence of which was obtained by fitting the data with generalized Laguerre polynomials. Subsequently, several groups[71, 93, 94] have performed PSA for determining the $I = 0$ scattering amplitudes below 800 MeV, accompanied with experimental development.

Evidence for narrow resonances in the $I = 1$ state has been reported in the $^3\mathrm{He}(p, d)X$ reaction data[95, 96] and also in the KEK A_y-data[97] at $\sqrt{s} = 2160$ and 2190 MeV, which were analyzed by Kobayashi et al.[98] and our group[72]. A narrow resonance-like peak around at 630 MeV has been observed in the $I = 0$ total cross section difference $\Delta\sigma_L{}^0$ in the polarized n-p experiment[99]. A possible narrow $I = 0$ resonance with $J^P = 1^-$ and $M = 2168$ MeV/c^2, which corresponds to $T_L = 625$ MeV, was suggested by Hoshizaki[94] on the basis of the neutron-proton PSA between 430 and 800 MeV.

Recently plentiful data on spin correlation parameters in the n-p scattering have been presented at $T_L = 635, 647, 790$ and 800 MeV at LAMPF, and above 800 MeV at Saclay.

The purpose of this article is to present the result of the single-energy PSA at 10 energy-points between 500 and 1090 MeV, where relatively plentiful data have been accumulated. Here the $I = 1$ amplitudes are fixed on the values determined by the PSA of p-p scattering at the same energies[13]. We also discuss the result of the semi-energy dependent PSA of n-p scattering between 500 and 800 MeV, which were executed while carefully considering the $\Delta\sigma_L$-data given by Beddo et al.[99].

A narrow resonance-like structure in the $^1P_1$ wave is not found in the solutions of the single-energy analyses of the overall data using the smoothed pseudo-data of forward observables (σ_t, σ_r, $\Delta\sigma_L$ and $\Delta\sigma_T$), but it is detected in the solution of the semi-energy dependent PSA. Also the possibility of counter-clockwise behaviour of the $^3D_1$ amplitude cannot be excluded in the present situation of experimental data.

In subsection 3.4.2, we perform an evaluation of an inelastic effect of n-p scattering, in paticular, the $I = 0$ inelastic cross section. In subsection 3.4.3, the experimental data used in the present analyses are reported. In subsection 3.4.4, the results of the single-energy PSA of n-p scattering between 500 and 1090 MeV are shown, and subsection 3.4.5 is devoted to

reporting the semi energy dependent PSA from 500 to 800 MeV and concluding remarks.

3.4.2 Inelastic effect in *n-p* scattering

Total inelastic *n-p* cross section, which is hereafter called *n-p* reaction cross section, $\sigma_r(np)$ should be evaluated with extreme accuracy, since it plays a principal role for the determination of the absorption effect, i.e., the imaginary phase-shifts in the PSA of elastic *n-p* scattering. VerWest and Arndt[100], and Bystricky et al.[92] extracted σ_r from experimental data of nucleon-nucleon inelastic scattering due to charge independence. There is a noticeable difference between their evaluations of the $I = 0$ reaction cross section ($\sigma_0{}^r$), which has been discussed by Bystricky et al.[92]. We give this problem our careful consideration below.

The total cross sections of *p-p* and *n-p* scatterings, $\sigma_t(pp)$ and $\sigma_t(np)$, are given as

$$\sigma_t(pp) = \sigma_1, \tag{3.23}$$

$$\sigma_t(np) = \frac{1}{2}(\sigma_1 + \sigma_0), \tag{3.24}$$

where σ_1 and σ_0 are the total cross sections in the $I = 1$ and $I = 0$ isospin states, respectively. Hence we have the $I = 1$ and $I = 0$ reaction cross sections ($\sigma_1{}^r$ and $\sigma_0{}^r$) from the *p-p*- and *n-p*-reaction cross section ($\sigma_r(pp)$ and $\sigma_r(np)$) as follows:

$$\sigma_1{}^r = \sigma_r(pp), \tag{3.25}$$

$$\sigma_0{}^r = 2\sigma_r(np) - \sigma_r(pp). \tag{3.26}$$

The one-pion production processes supply most of the contribution to σ_r below 1 GeV, whose effect occupies about 98% of σ_r at 1 GeV. The above relations hold also for one-pion production processes,

$$\sigma_1(NN \to NN\pi) = \sigma(pp \to pp\pi^0) + \sigma(pp \to pn\pi^+), \tag{3.27}$$

$$\begin{aligned}\sigma_0(NN \to NN\pi) = {} & 2[\sigma(np \to np\pi^0) + \sigma(np \to nn\pi^+) + \sigma(np \to pp\pi^-)] \\ & -[\sigma(pp \to pp\pi^0) + \sigma(pp \to pn\pi^+)].\end{aligned} \tag{3.28}$$

These relations hold for multi-pion production processes.

By means of the isospin invariance, the following relations among inelastic total cross sections are derived as

$$\sigma(np \to pp\pi^-) = \sigma(np \to nn\pi^+), \tag{3.29}$$

$$2\sigma(np \to pp\pi^-) + \sigma(pp \to np\pi^+) = 2[\sigma(pp \to pp\pi^0) + \sigma(np \to np\pi^0)]. \tag{3.30}$$

Using the relations (3.28), (3.29) and (3.30), we have

$$\sigma_0(NN \to NN\pi) = 3[2\sigma(np \to pp\pi^-) - \sigma(pp \to pp\pi^0)]. \tag{3.31}$$

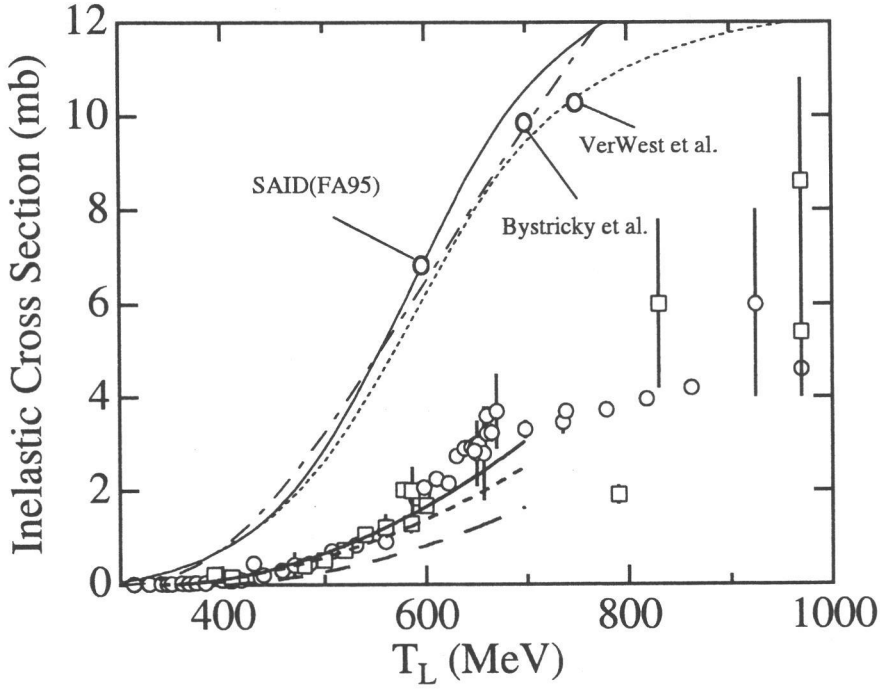

Figure 3.7: The experimental data of $\sigma(np \to NN\pi^{\pm})$ and $\sigma(pp \to pp\pi^0)$ are shown by the symbols □, and ○, respectively, where $\sigma(np \to NN\pi^{\pm})$ represents $\sigma_0(np \to nn\pi^+) + \sigma_0(np \to pp\pi^-)$. The solid and dotted lines indicate the ones obtained by χ^2-fit to the data of $\sigma(np \to NN\pi^{\pm})$ and $\sigma(pp \to pp\pi^0)$ below 600MeV, respectively. The broken line is the evaluated $I = 0$ reaction cross section ${\sigma_0}^r$, which is obtained by Eq.(3.31), i.e., three times of the difference between the solid and the dotted lines. The values of $\sigma_r(np)$ evaluated by Bystricky et al.[92], VerWest et al.[100], and Arndt(SAID95)[71]) are also given.

VerWest and Arndt concluded that ${\sigma_0}^r$ is essentially zero below 1 GeV because the right-hand side of Eq.(3.31) is equal to zero due to the experimental data on $\sigma(np \to pp\pi^-)$ and $\sigma(pp \to pp\pi^0)$. On the other hand, Bystricky et al. suggested a possible violation of the relation(3.30) based on experimental data and gave an evaluation of ${\sigma_0}^r$ in the energy range below 4.2 GeV using the sum of individual exclusive channels and direct measurements. In their evaluation, $\sigma_r(np)$ and ${\sigma_0}^r$ are equal to about 6 mb and about 1 mb at 600 MeV, respectively.

It is difficult to consider the violation of isospin invariance. We plot the experimental data on $\sigma(np \to NN\pi^{\pm})$ and $\sigma(pp \to pp\pi^0)$ in Fig. 3.7, the difference of which should be equal to $\sigma_0(NN \to NN\pi)/3$ from Eq.(3.31). Here $\sigma_0(np \to NN\pi^{\pm})$ represents $\sigma_0(np \to nn\pi^+) + \sigma_0(np \to pp\pi^-)$. The solid and the dotted lines are obtained by the χ^2-fit to the data on $\sigma(np \to NN\pi^{\pm})$ and $\sigma(pp \to pp\pi^0)$ below 600 MeV with the 2nd order polynomials. The data on $\sigma(pp \to pp\pi^0)$ are larger than the extrapolated solid line at $T_L = 600 - 670$ MeV as is seen in Fig. 3.7. But we do not know any threshold effects which cause such radical energy-dependence in this energy region. If these lines given by interpolation of the data below 600 MeV are reliable, the $I = 0$ reaction cross section is equal to three times the

Table 3.8: The total cross section and the partial total cross sections in $^3S_1$, $^1P_1$, $^3D_1$ and $^3D_2$ states calculated with $g_{\sigma NN} = 0.82$ at each energy.

P_L [GeV/c]	$\sigma_t[\mu b]$	$\sigma\left(^3S_1\right)(\mu b)$	$\sigma\left(^1P_1\right)(\mu b)$	$\sigma\left(^3D_1\right)(\mu b)$	$\sigma\left(^3D_2\right)(\mu b)$
1.3	3.56	2.77	2.53×10^{-4}	0.78	3.84×10^{-5}
1.4	14.25	11.11	1.80×10^{-3}	3.12	1.97×10^{-4}
1.5	44.31	34.47	8.06×10^{-3}	9.74	4.23×10^{-4}
1.6	96.13	74.37	2.60×10^{-2}	21.41	4.64×10^{-4}

difference between the solid line and dotted line, which is shown by the broken line in Fig. 3.7. From this evaluation, ${\sigma_0}^r \sim 1.5$ mb at 600 MeV, which is about 23 % of $\sigma_r(np)$. In this case, we have the possibility that the $I = 0$ inelastic resonance has a width narrower than that predicted by Hoshizaki[94]. This evaluation of ${\sigma_0}^r$ will be compared with the result of our PSA of n-p scattering later.

An absorption effect in n-p elastic scattering should appear in the lower partial amplitudes above the threshold energy and exponentially dump with increasing angular momentum, because of the main contribution of one-pion production process to σ_r. Bannwarth et al.[101], however, observed a strong anisotropic angular distribution in the $np \to NN\pi^{\pm}$ reaction at $T_L = 460 - 560$ MeV, and manifested a non-negligible contribution from the $^3D_1$-initial state. A similar anisotropic distribution was also obtained in the $np \to pp\pi^-$ reaction at 443 MeV[102]. Thus, we should consider the absorptions of $^3S_1$, $^1P_1$ and $^3D_1$ in the PSA of n-p scattering around at 600 MeV.

Above 1 GeV, a threshold effect of the $np \to np(\pi\pi)^0$ reaction may have a considerable contribution to ${\sigma_0}^r$, which is called the ABC-effect. The ABC-peaks were observed in the measurement of $np \to dX$ reaction at 1.9 GeV/c($T_L = 1180$ MeV), which was provided by Plouin et al.[103]. On the other hand, such strong enhancements were not observed in the subsequent measurement of the $np \to d(\pi\pi)^0$ reaction at 1.46 GeV/c($T_L = 795$ MeV)[104]. The $\Delta\Delta$ model[105] and the double-nucleon exchange model[106] have been proposed to explain the ABC-effect in the differential cross section for $np \to dX$ at several deuteron angles, but their predictions are in disagreement with the data.

We calculated the differential cross section for the $np \to d(\pi\pi)^0$ with the $np \to \sigma d$ model[107], where the scattering amplitudes were assumed to be a product of the Born amplitude of $np \to \sigma d$ and the decay amplitude of $\sigma \to (\pi\pi)^0$. Our calculated differential cross section reproduces the data at 1.46 GeV/c quite well. However the ABC-peaks in the differential cross section data at 1.9 GeV/c and the predictions by our model coincide at the deuteron lab angle of 1.2°, but do not coincide at the larger angles. We need some corrections of our $np \to \sigma d$ model by other models, such as the $\Delta\Delta$ model.

In Table 3.8, we give the total cross sections of $np \to d(\pi\pi)^0$ and their partial cross sections in $^3S_1$, $^1P_1$, $^3D_1$ and $^3D_2$ states calculated by our model for reference. As is seen in this table, the partial cross section in the $^3S_1$ state is dominant, and the one in the $^3D_1$ state is secondarily large.

3.4.3 Experimental data

We execute the single-energy PSA of the experimental data at T_L = 500, 580, 630, 730, 800, 830, 870, 930, 990 and 1090 MeV in subsection 3.4.4. The following criteria are adopted on the selection of data base at each energy.

(1) Except for the forward observables, we take the data within the energy bin $\Delta T_L = \pm 20$ MeV at $T_L \leq 800$ MeV, and $\Delta T_L = \pm 30$ MeV at $T_L > 800$ MeV.

(2) Some old data are omitted.

(3) For forward observables, we make the data base in the following:

(a) The σ_r-values evaluated by Bystricky et al.[92] are used as the data below 800 MeV which are almost equal to the values given by VerWest and Arndt[100] in this energy range, and their error bars are taken as ± 0.1 mb. As the input data on σ_r above 830 MeV, we take the values which are given by interpolation of the experimental data using the spline-function. Their errors are taken as 10% of the used σ_r-values.

(b) The energy dependences of σ_t, $\Delta\sigma_L$ and $\Delta\sigma_T$ data are smoothed by the spline-function method. Their error bars in the present analysis at each energy are 1.5 times the average of the experimental error bars of the data used for interpolation.

(c) The real to imaginary ratio of forward amplitudes α, and the forward amplitudes $\mathrm{Re}F_2$ and $\mathrm{Re}F_3$ evaluated by dispersion relations[36], are also used in the analysis.

The number of the data used in the single-energy PSA at each energy is listed in Table 3.9.

The data references and their laboratories are given in subsection 3.4.6. It is especially noted that there are little experimental data on $d\sigma/d\Omega$ in the range of c.m.s. scattering angle $\theta_c = 60° - 90°$, except for those at 500, 630 and 800 MeV. We supply the deficiency of data on $d\sigma/d\Omega, P, A_{NN}, A_{LL}$ and A_{SL} at some energy-points with pseudo-data, whose numbers are shown in the parentheses. Those pseudo-data were presented by means of interpolating the experimental data on their energy dependences with the spline-function method.

3.4.4 Phase-shift analysis of *n-p* scattering

We take the representation of S-matrices proposed by Arndt et al.[66] as follows:

$$S_{l,J} = \frac{1 + iK_{l,J}}{1 - iK_{l,J}}. \tag{3.32}$$

For the singlet states and the uncoupled triplet states, K-matrices are given by

$$K_{l,J} = \tan\delta_{l,J} + i\tan^2\rho_{l,J}, \tag{3.33}$$

where l and J are the orbital and the total angular momenta, respectively. The usual reflection parameters $\eta_{l,J}$ are related to $(\delta_{l,J}, \rho_{l,J})$ by

Table 3.9: The observables and their numbers of the experimental data used in the single energy phase-shift analysis at each energy. The references are given in subsection 3.4.6.

T_L(MeV)	500	580	630	730	800	830	870	930	990	1090
Forward Obs.[a)]	7(3)	7(3)	7(3)	7(3)	7(3)	7(4)	7(4)	7(4)	7(4)	7(4)
$d\sigma/d\Omega$	383	335(25)	457	185(27)	318	410	138(25)	137(25)	254(25)	199
P	88	46(5)	102	51(7)	173	209	203(5)	218	76	58
R	4	3	4		13	13				
A	3	4	4		11	11				
R'	4		4		13	13				
A'	3		4		12	12				
D	3	3	12		11	18	7	9	4	4
D_{LS}					2	5	4	4	4	3
A_{NN}	14(14)	30(15)	14(14)	22(15)	58	120	95	77	40	43
A_{LL}	21	12(12)	33	14(14)	48	56	51	30	44	44
A_{SL}	20	7(7)	20	15(7)	57	64	37	29	43	37
$C_{\sigma\sigma}$	21		22		20					
K_{NN}	54	5	33		38	12	7	9	4	4
K_{LL}	7		39		39					
K_{LS}	18		39		41	5	4	4	4	3
K_{SL}	10	3	39		42	3				
K_{SS}	25	4	39		44	8	4	4	4	3
H_{LLN}					2	5	4	4	4	3
H_{LNS}					2	5	4	4	4	3
Total	685	459	872	294	951	976	565	536	492	411

a) Forward Obs.: $\sigma_t, \sigma_r, \Delta\sigma_T, \Delta\sigma_L, \alpha$, Re$F_2$, Re$F_3$

$$\eta_{l,J}{}^2 = \frac{1 + |K_{l,J}|^2 - 2\mathrm{Im}K_{l,J}}{1 + |K_{l,J}|^2 + 2\mathrm{Im}K_{l,J}}. \tag{3.34}$$

For the coupled triplet states between $l = J \pm 1$, K matrices are defined by

$$K_{l,J} = \begin{bmatrix} K_- & K_0 \\ K_0 & K_+ \end{bmatrix} + i \begin{bmatrix} \tan^2\rho_- & \tan\rho_-\tan\rho_+ \\ \tan\rho_-\tan\rho_+ & \tan^2\rho_+ \end{bmatrix}, \tag{3.35}$$

$$\begin{aligned} K_\pm &= \frac{\sin(\delta_{J+1,J} + \delta_{J-1,J}) \pm \cos 2\epsilon_J \sin(\delta_{J+1,J} - \delta_{J-1,J})}{\cos(\delta_{J+1,J} + \delta_{J-1,J}) + \cos 2\epsilon_J \cos(\delta_{J+1,J} - \delta_{J-1,J})}, \\ K_0 &= \frac{\sin\epsilon_J}{\cos(\delta_{J+1,J} + \delta_{J-1,J}) + \cos 2\epsilon_J \cos(\delta_{J+1,J} - \delta_{J-1,J})}. \end{aligned} \tag{3.36}$$

The partial-wave amplitudes with $J > J_0$, where $J_0 = 7$ below 630 MeV, 8 at 730 – 990 MeV and 9 at 1090 MeV respectively, are calculated by the one-pion exchange contribution with $g^2_{\pi NN} = 13.75$, where the isospin invariance is assumed. The S-matrices are related to the partial wave amplitudes $h_{l,J}$ as follows:

$$h_{l,J} = \frac{1}{2i}(S_{l,J} - 1). \tag{3.37}$$

The five Goldberger-Grissaru-MacDowell-Wong s-channel helicity amplitudes[108] defined by the partial wave amplitudes are used.

A best fit solution is obtained by varying the free parameters ($\delta_{l,J}$ and $\rho_{l,J}$) so as to minimize the χ^2-value:

$$\chi^2 = \sum_{i,j} \left[\left((1+\epsilon_j)\theta^{\rm ex}_{i,j} - \theta^{\rm th}_{i,j} \right) / \Delta\theta^{\rm ex}_{i,j} \right]^2 + \sum_j \left(\frac{\epsilon_j}{\Delta\epsilon_j} \right)^2 , \tag{3.38}$$

where $\theta^{\rm ex}_{i,j}$ is the experimental datum of observable i for the jth experiment with the experimental error $\Delta\theta^{\rm ex}_{i,j}$ and $\theta^{\rm th}_{i,j}$ is the theoretical value. Here $N_j = (1+\epsilon_j)$ is the renormalization parameter assigned to the data of the jth group. N_j is used as a free parameter only for some data on the differential cross section where extreme differences among the data groups exist.

The n-p scattering amplitude is composed of the $I = 1$ amplitude and the $I = 0$ amplitude. The $I = 1$ amplitude is fixed to the solution obtained by the previous PSA of p-p scattering[13], and the $I = 0$ amplitude is searched by the above mentioned method.

The energy point $T_L = 500$ MeV is chosen as a starting point of PSA since there is a fairly good accumulation of experimental data. Each of the obtained solutions is followed stepwise to higher energies by using the solution as the starting parameters for the search at neighbouring energies. Finally the solutions which match with the established amplitudes well at lower energies are taken as acceptable. The obtained solutions of the present single-energy PSA from 500 to 1090 MeV are listed in Table 3.10.

A strong correlation is found in data fitting between $d\sigma/d\Omega$ and A_{NN} around at $\theta_c = 90°$, which is considered to be brought about from the terms $4|\phi_5|^2$ in the $d\sigma/d\Omega$-expression and the term $2|\phi_5|^2$ in the A_{NN}-expression, respectively.

Some problems of the data used here are found by the analyses as follows:

- 580 MeV: the data on $d\sigma/d\Omega$[Ref. SI(89)] at small angles are larger by $1-2$ mb than our predictions, which may be inconsistent with the forward data.
- 630 MeV: the data on $d\sigma/d\Omega$[Ref. SH(74)] in the range $\theta_c = 95° - 180°$ are extremely inconsistent with the data given by the other groups, and therefore they have been multiplied by the renormalization factor $N = 1.4$ in our PSA.
- 800 MeV: the data on $d\sigma/d\Omega$[Ref. SH(74)] are smaller on the whole than the ones of the other groups, and their renormalization factor $N = 1.4$.
- 990 MeV: our predictions of $d\sigma/d\Omega$ around at 90° are located nearly in the center of the data varying widely, which are caused by determining $|\phi_5|^2$ with the A_{NN}-data for the above mentioned reason.

The calculated values of $d\sigma/d\Omega$ at $T_L = 580$, 870, 930 and 1090 MeV are larger around at $\theta_c = 90°$ than the pseudo-data given by the spline-function method, but they are more reliable than the pseudo-data for the reason mentioned above about ϕ_5 amplitudes.

The present solution has the following characteristics and some of them are different from the ones given by SAID[71].

(1) At $T_L \gtrsim 800$ MeV our predicted values of σ_r are near to those of SAID(FA95), and the slope of our obtained σ_r is more gentle than the one predicted by Bystricky et al.[92].

(2) Our σ_r-values above 800 MeV, which are a little larger than SAID's, result in the relatively large absorption of $^3D_2$-wave in the present solution. The reason of our searching $\rho_{l,J}$ of $l = 2$ was discussed in the section 3.4.2.

Table 3.10: The solutions obtained by single-energy phase-shift analysis (sol. A).

T_L(MeV)	500		580	
Partial waves	δ	ρ	δ	ρ
$^3S_1$	− 11.44±0.09	0.41±0.09	− 9.86±0.10	1.61±0.08
ϵ_1	6.54±0.09		6.37±0.03	
$^1P_1$	− 37.37±0.09	13.83±0.13	− 40.83±0.03	15.20±0.05
$^3D_1$	− 29.66±0.19	0.59±0.14	− 29.26±0.15	5.14±0.05
$^3D_2$	18.62±0.07	0.42±0.17	17.69±0.01	0.64±0.03
$^3D_3$	4.12±0.05	0.05±0.10	5.86±0.03	2.24±0.05
ϵ_3	8.67±0.03		8.36±0.01	
$^1F_3$	− 6.52±0.06		− 6.73±0.03	
$^3G_3$	− 6.54±0.05		− 7.86±0.02	
$^3G_4$	8.43±0.04		9.14±0.01	
$^3G_5$	− 0.29±0.03		− 0.52±0.02	
T_L(MeV)	630		730	
Partial waves	δ	ρ	δ	ρ
$^3S_1$	− 19.44±0.19	3.28±0.25	− 21.01±0.31	6.01±0.35
ϵ_1	6.11±0.11		4.17±0.07	
$^1P_1$	− 42.09±0.14	17.04±0.31	− 45.50±0.22	23.01±0.19
$^3D_1$	− 29.27±0.19	12.46±0.20	− 30.97±0.19	11.71±0.16
$^3D_2$	16.14±0.12	0.51±0.32	15.37±0.06	5.99±0.19
$^3D_3$	3.83±0.07	2.16±0.47	2.81±0.04	0.51±0.06
ϵ_3	7.16±0.06		4.92±0.02	
$^1F_3$	− 8.89±0.04		− 8.24±0.02	0.62±0.12
$^3G_3$	− 4.14±0.08		− 5.74±0.09	
$^3G_4$	10.13±0.09		10.99±0.07	
$^3G_5$	0.16±0.06		− 0.44±0.03	
T_L(MeV)	800		830	
Partial waves	δ	ρ	δ	ρ
$^3S_1$	− 27.27±0.06	8.19±0.05	− 30.86±0.14	0.18±0.15
ϵ_1	9.02±0.01		6.93±0.16	
$^1P_1$	− 41.83±0.17	26.15±0.23	− 37.73±0.21	27.41±0.21
$^3D_1$	− 32.03±0.11	4.89±0.11	− 31.16±0.22	6.80±0.25
$^3D_2$	8.95±0.14	3.76±0.14	10.40±0.15	10.58±0.15
$^3D_3$	2.78±0.06	9.61±0.08	1.75±0.09	4.89±0.14
ϵ_3	7.56±0.05		6.61±0.06	
$^1F_3$	− 10.42±0.11	9.20±0.09	− 10.43±0.12	9.73±0.10
$^3G_3$	− 4.98±0.05		− 6.88±0.07	
$^3G_4$	10.45±0.07		10.32±0.07	
$^3G_5$	0.26±0.04		− 0.36±0.06	
ϵ_5			3.07±0.03	
$^1H_5$			− 2.54±0.07	
$^3I_5$			− 2.80±0.05	
$^3I_6$			5.19±0.05	
$^3I_7$			− 1.23±0.05	

Table 3.10: (continued)

T_L(MeV)	870		930	
Partial waves	δ	ρ	δ	ρ
$^3S_1$	− 32.17±0.04	5.02±0.07	− 34.37±0.15	4.03±0.16
ϵ_1	8.74±0.24		5.89±0.23	
$^1P_1$	− 42.46±0.25	23.99±0.31	− 42.33±0.29	27.02±0.30
$^3D_1$	− 35.96±0.27	3.02±0.28	− 32.82±0.20	0.13±0.24
$^3D_2$	8.73±0.19	13.31±0.16	10.38±0.22	21.02±0.17
$^3D_3$	1.00±0.02	0.19±0.20	1.29±0.16	10.06±0.16
ϵ_3	4.59±0.08		3.18±0.10	
$^1F_3$	− 11.67±0.19	0.14±0.16	− 10.40±0.16	5.00±0.14
$^3G_3$	− 7.22±0.10		− 7.92±0.12	
$^3G_4$	9.96±0.09		8.62±0.10	
$^3G_5$	− 1.30±0.07		− 0.13±0.08	
ϵ_5	3.85±0.05		3.40±0.06	
$^1H_5$	− 3.17±0.10		− 2.41±0.10	
$^3I_5$	− 1.32±0.01		− 1.47±0.10	
$^3I_6$	5.24±0.07		5.03±0.08	
$^3I_7$	− 0.83±0.05		− 0.77±0.08	
T_L(MeV)	990		1090	
Partial waves	δ	ρ	δ	ρ
$^3S_1$	− 41.37±0.02	0.29±0.34	− 42.39±0.38	0.93±0.61
ϵ_1	6.62±0.08		3.32±0.22	
$^1P_1$	− 40.20±0.15	34.96±0.08	− 34.52±0.40	32.87±0.24
$^3D_1$	− 35.96±0.02	4.54±0.05	− 35.08±0.40	16.57±0.31
$^3D_2$	0.73±0.04	15.25±0.13	7.14±0.30	21.75±0.19
$^3D_3$	1.98±0.02	13.53±0.02	− 5.23±0.30	21.08±0.19
ϵ_3	3.61±0.01		3.35±0.12	
$^1F_3$	− 10.71±0.05	1.29±0.09	− 11.38±0.13	1.44±0.19
$^3G_3$	− 7.45±0.02		− 12.76±0.27	
$^3G_4$	10.69±0.03		4.57±0.11	
$^3G_5$	− 0.51±0.02		− 1.73±0.14	
ϵ_5	3.85±0.02		3.00±0.04	
$^1H_5$	− 6.78±0.04		− 4.70±0.09	
$^3I_5$	− 2.06±0.02		− 3.87±0.15	
$^3I_6$	6.38±0.02		5.28±0.07	
$^3I_7$	− 1.39±0.02		1.01±0.09	

Table 3.11: The observables and their numbers of the experimental data used in the semi-energy dependent phase-shift analysis at each energy. The data references are given in the section 3.4.6.

T_L(MeV)	500	560	580	630	680	740
Forward Obs.[a)]	7(4)	7(4)	7(4)	7(4)	7(4)	7(4)
$d\sigma/d\Omega$	383	367(28)	335(25)	404	281(28)	388(25)
P	88	50	46(5)	102	80	85
R	4		3	4	4	
A	3		4	4	4	
R'	4			4	4	
A'	3			4	4	
D	3		3	12	8	
A_{NN}	14(14)	29(14)	29(14)	14(14)	29(14)	30(14)
A_{LL}	21	8(8)	12(12)	33	11(11)	35(14)
A_{SL}	20	9(9)	7(7)	20	9(9)	36(7)
$C_{\sigma\sigma}$	21			22		20
K_{NN}	54		5	33		36
K_{LL}	7			39		39
K_{LS}	18			39		39
K_{SL}	10		3	39		42
K_{SS}	25		4	39		42
Total	685	470	458	819	441	799

a) Forward Obs.: $\sigma_t, \sigma_r, \Delta\sigma_T, \Delta\sigma_L, \alpha$, Re$F_2$, Re$F_3$

(3) The absorption of $^1P_1$-wave is relatively large over the whole energy range.

3.4.5 Discussions and concluding remarks

The narrow resonance of $J^P = 1^-$ ($M = 2168$ MeV, $\Gamma = 25$ MeV, $\Gamma_{el}/\Gamma = 0.2$) was predicted by Hoshizaki[94] in an appearance as a counterclock-wise behaviour of the $^1P_1$ partial wave amplitude between 500 and 700 MeV. In the single-energy PSA (SE-PSA) reported in the previous subsection, there are only two energy points in the related energy region, which is too poor for observation of the above behaviour.

Next we make a semi-energy dependent PSA(ED-PSA) from 500 MeV to 740 MeV by using the data base as shown in Table 3.11. The reason for naming this analysis the ED-PSA is that the energy dependences of the experimental data on $d\sigma/d\Omega$ and A_{NN} are regarded as important, so that they are evaluated by the spline-function and reflected in the energy dependence of a solution of partial amplitudes. The data base is made by the next processing.

(1) The energy bin of the $d\sigma/d\Omega$-data selection is 20 MeV at each energy besides $T_L = 740$ MeV where it is 30 MeV.

(2) The energy bins of the data selection except for $d\sigma/d\Omega$-data are 20, 20, 20, 20, 40 and 50 MeV at 500, 560, 580, 630, 680 and 740 MeV, respectively.

(3) We add the pseudo-data on $d\sigma/d\Omega$ and A_{NN} obtained by spline-interpolation of their experimental data on the energy dependences to regard their energy dependences as important.

(4) In order to make up for the wants of experimental data on P, A_{LL} and A_{SL} at several energy-points, the pseudo-data are supplied by means of the spline-interpolation of experimental data on their energy dependences. The number of pseudo-data are given in the parentheses.

(5) The A_{NN}-data of Ref. LE(88) at 744 MeV are excluded in the data base because they are not compatible with the other data on the energy dependence.

(6) The error bars of σ_r presented by Bystricky et al.[92] are taken as follows,

(Case I) $\Delta\sigma_r = \pm 0.1$ mb, which is the same value as in the single-energy PSA,

(Case II) $\Delta\sigma_r = \pm 0.5$ mb.

If the starting values of the free parameters with the relatively small χ^2-value are taken in PSA, the solution in the χ^2-minimization might be trapped in a local valley with high possibility. To avoid such a trouble, the solution of SE-PSA at 500 MeV is used as the starting values of our ED-PSAs at 560 and 580 MeV, and the solution of SE-PSA at 800 MeV as the starting values at 680 and 740 MeV. The solution at 580 MeV is taken as the starting values at 630 MeV. At 500 and 800 MeV, we obtained stable solutions as reported in the previous section. We finally take the solution as acceptable when they can match the established amplitudes at 500 and 800 MeV well.

Hereafter we call the solution of the SE-PSA Sol. A, the ED-PSA of the above mentioned data base with Case I sol. B and the one with Case II sol. C. The phase shifts of sol. B and C are tabulated in Table 3.12. The forward observables predicted by Sols. A, B and C are shown in Fig. 3.8 with the experimental data. The calculated values of $d\sigma/d\Omega$ and A_{NN} of sol. B are shown in Fig. 3.9 for references.

In Fig. 3.8, the calculated $\Delta\sigma_L$ in Sols.A and B refuse to fit to the data given by Beddo et al.[99] around 600 MeV due to the fitting of the σ_r-data given by Bystricky et al.[92] with the error bar of $\sigma_r \pm 0.1$ mb. sol. C, where the error bar of σ_r is ± 0.5 mb, represent Beddo's $\Delta\sigma_L$-data. In sol. C, the calculated value of ${\sigma_0}^r$ is 1.37 mb at 580 MeV, which is about 25% of $\sigma_r(np)$ datum, and is in good agreement with our previous evaluation in subsection 3.4.2.

The dip structure of $\Delta\sigma_T$ in Sols.B and C in the range $500 - 630$ appears owing to the large errors of $\Delta\sigma_T$, and seems to be not worthy of notice.

The Argand diagrams of sol. A, B, and C are given in Fig. 3.10 for the waves of ${}^1P_1$ and ${}^3D_1$.

The narrow resonance-like structure of the ${}^1P_1$ state is observed only in sol. C, which is strongly related to the $\Delta\sigma_L$-data presented by Beddo et al.[99], and its predicted values of the $I = 0$ inelastic cross section are not inconsistent with the values which are evaluated by using the experimental data of inelastic cross sections at lower energies with the isospin invariance.

In the resonance structure appeared in $\Delta\sigma_T = -4\sqrt{\pi}\mathrm{Im}\phi_2(0)$, a resonance of the state without wave coupling has a bump structure and the one of the state with wave coupling has

Table 3.12: (a) The solutions obtained by the semi-energy dependent phase-shift analysis (sol. B).

T_L(MeV)	560		580	
Partial waves	δ	ρ	δ	ρ
$^3S_1$	-14.36 ± 0.24	0.12 ± 0.23	-10.62 ± 0.25	7.84 ± 0.20
ϵ_1	4.67 ± 0.14		6.29 ± 0.14	
$^1P_1$	-38.53 ± 0.10	14.05 ± 0.13	-39.61 ± 0.13	15.80 ± 0.17
$^3D_1$	-30.17 ± 0.36	19.57 ± 0.20	-33.26 ± 0.35	10.68 ± 0.25
$^3D_2$	19.43 ± 0.09	0.06 ± 0.22	16.94 ± 0.11	0.67 ± 0.20
$^3D_3$	2.24 ± 0.10	0.32 ± 0.18	5.11 ± 0.09	0.21 ± 0.18
ϵ_3	7.56 ± 0.03		8.14 ± 0.04	
$^1F_3$	-6.56 ± 0.06		-7.02 ± 0.08	
$^3G_3$	-5.35 ± 0.04		-8.64 ± 0.10	
$^3G_4$	9.76 ± 0.05		10.17 ± 0.05	
$^3G_5$	-0.39 ± 0.07		0.35 ± 0.06	
T_L(MeV)	630		680	
Partial waves	δ	ρ	δ	ρ
$^3S_1$	-17.21 ± 0.08	2.74 ± 0.08	-22.07 ± 0.22	4.96 ± 0.20
ϵ_1	7.11 ± 0.12		2.78 ± 0.19	
$^1P_1$	-42.00 ± 0.14	17.34 ± 0.18	-46.06 ± 0.20	23.16 ± 0.25
$^3D_1$	-31.36 ± 0.19	12.71 ± 0.10	-32.24 ± 0.36	19.43 ± 0.23
$^3D_2$	15.43 ± 0.10	0.16 ± 0.19	18.19 ± 0.13	0.52 ± 0.24
$^3D_3$	3.66 ± 0.07	0.69 ± 0.12	0.93 ± 0.13	0.03 ± 0.20
ϵ_3	7.59 ± 0.04		6.89 ± 0.06	
$^1F_3$	-9.17 ± 0.08		-9.05 ± 0.11	3.04 ± 0.11
$^3G_3$	-3.85 ± 0.05		-8.33 ± 0.12	
$^3G_4$	10.77 ± 0.06		9.14 ± 0.07	
$^3G_5$	0.30 ± 0.04		-0.83 ± 0.08	
T_L(MeV)	740			
Partial waves	δ	ρ		
$^3S_1$	-24.15 ± 0.20	9.01 ± 0.18		
ϵ_1	7.18 ± 0.15			
$^1P_1$	-43.74 ± 0.16	25.71 ± 0.16		
$^3D_1$	-32.21 ± 0.23	13.48 ± 0.22		
$^3D_2$	12.51 ± 0.14	0.29 ± 0.19		
$^3D_3$	2.28 ± 0.11	0.20 ± 0.18		
ϵ_3	7.33 ± 0.04			
$^1F_3$	-8.83 ± 0.08	6.71 ± 0.09		
$^3G_3$	-6.68 ± 0.09			
$^3G_4$	10.00 ± 0.06			
$^3G_5$	-0.55 ± 0.07			

Table 3.12: (b) The solutions obtained by the semi-energy dependent phase-shift analysis (sol. C).

T_L(MeV)	500		560	
Partial waves	δ	ρ	δ	ρ
$^3S_1$	-11.10 ± 0.23	0.32 ± 0.81	-15.68 ± 0.25	0.18 ± 0.23
ϵ_1	6.02 ± 0.16		4.17 ± 0.14	
$^1P_1$	-38.54 ± 0.12	16.22 ± 0.36	-38.03 ± 0.10	18.13 ± 0.13
$^3D_1$	-30.13 ± 0.14	5.57 ± 0.73	-30.38 ± 0.38	19.75 ± 0.20
$^3D_2$	17.78 ± 0.14	0.05 ± 4.14	19.16 ± 0.10	0.24 ± 0.23
$^3D_3$	3.30 ± 0.08	1.41 ± 0.66	2.42 ± 0.09	0.10 ± 0.20
ϵ_3	8.97 ± 0.06		7.77 ± 0.03	
$^1F_3$	-6.15 ± 0.07		-6.74 ± 0.06	
$^3G_3$	-5.94 ± 0.09		-5.90 ± 0.08	
$^3G_4$	8.11 ± 0.08		9.74 ± 0.04	
$^3G_5$	-0.60 ± 0.06		-0.48 ± 0.05	
T_L(MeV)	580		630	
Partial waves	δ	ρ	δ	ρ
$^3S_1$	-11.18 ± 0.15	7.72 ± 0.20	-16.24 ± 0.08	4.09 ± 0.08
ϵ_1	6.53 ± 0.02		5.29 ± 0.02	
$^1P_1$	-37.71 ± 0.05	23.52 ± 0.04	-44.48 ± 0.04	20.51 ± 0.06
$^3D_1$	-33.65 ± 0.25	9.50 ± 0.05	-32.17 ± 0.18	14.22 ± 0.06
$^3D_2$	15.40 ± 0.01	1.74 ± 0.03	16.29 ± 0.02	0.44 ± 0.03
$^3D_3$	4.58 ± 0.04	0.51 ± 0.10	3.61 ± 0.05	2.67 ± 0.08
ϵ_3	8.64 ± 0.04		7.64 ± 0.04	
$^1F_3$	-7.72 ± 0.02		-9.26 ± 0.03	
$^3G_3$	-8.18 ± 0.03		-3.86 ± 0.03	
$^3G_4$	10.26 ± 0.01		9.06 ± 0.01	
$^3G_5$	0.34 ± 0.05		0.19 ± 0.04	
T_L(MeV)	680		740	
Partial waves	δ	ρ	δ	ρ
$^3S_1$	-19.93 ± 0.21	3.72 ± 0.21	-25.15 ± 0.20	9.89 ± 0.18
ϵ_1	2.37 ± 0.19		8.01 ± 0.16	
$^1P_1$	-46.06 ± 0.19	19.83 ± 0.26	-42.78 ± 0.16	25.50 ± 0.17
$^3D_1$	-31.98 ± 0.36	20.02 ± 0.23	-31.28 ± 0.22	12.68 ± 0.23
$^3D_2$	19.10 ± 0.13	0.13 ± 0.26	11.75 ± 0.15	0.84 ± 0.20
$^3D_3$	0.64 ± 0.13	0.05 ± 0.22	2.85 ± 0.11	0.35 ± 0.19
ϵ_3	6.79 ± 0.06		7.68 ± 0.04	
$^1F_3$	-9.14 ± 0.11	0.75 ± 0.12	-8.96 ± 0.08	9.00 ± 0.08
$^3G_3$	-7.97 ± 0.12		-6.23 ± 0.09	
$^3G_4$	8.89 ± 0.07		10.36 ± 0.06	
$^3G_5$	-0.93 ± 0.08		-0.02 ± 0.06	

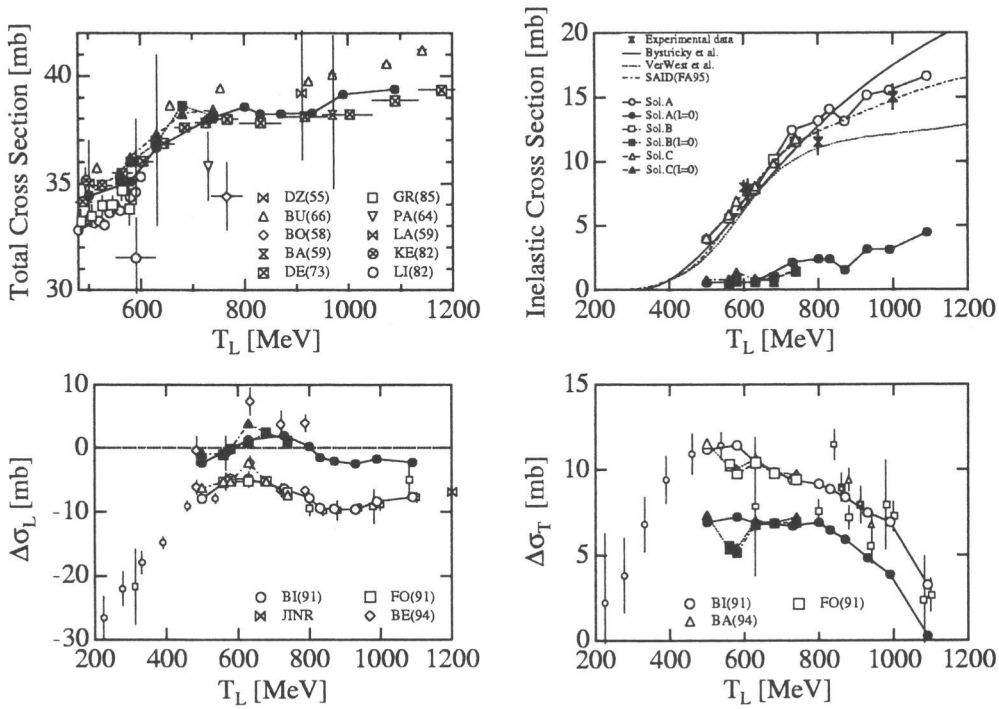

Figure 3.8: The experimental data of forward observables and the predictions of sol. A, sol. B and sol. C. The symbols ○, □ and △ show the calculated observables in Sols. A, B and C, respectively, and the symbols ●, ■ and ▲ their $I = 0$-component values, respectively. The other symbols give the experimental data.

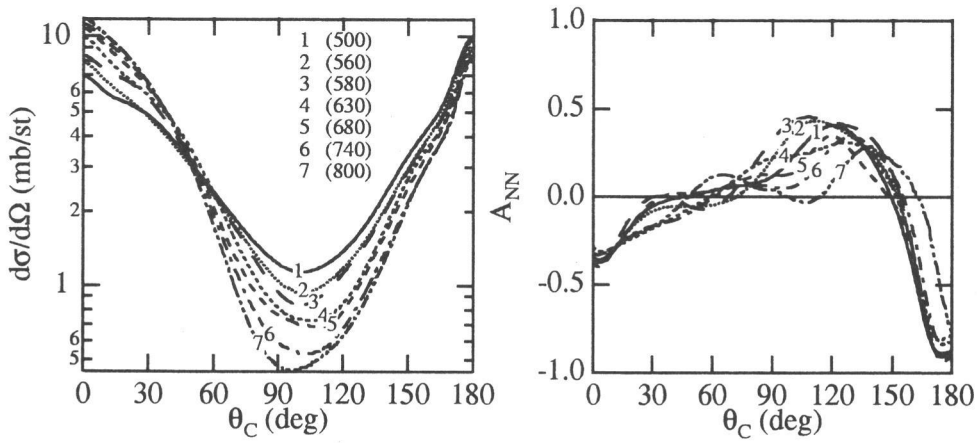

Figure 3.9: The erergy dependences of $d\sigma/d\Omega$ and A_{NN} calculated by Sol. B of the semi-energy dependent phase-shift analyses. The numbers[1−7] show the energy-points in the analyses, respectively.

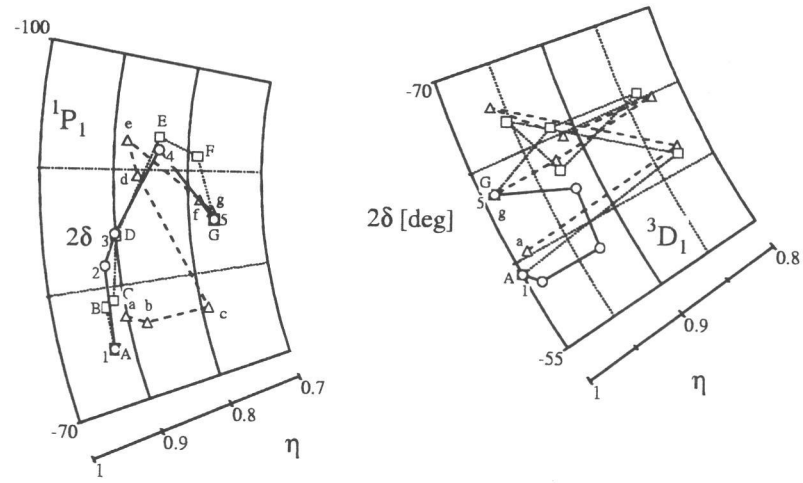

Figure 3.10: The Argand diagrams of $^1P_1$ and $^3D_1$-waves obtained by the present PSA. The symbols ○ [1−10] show the ten energy-points analyzed in Sol. A, the symbols □ [A−G] the seven energy points in Sol. B and the symbols △ [$a - g$] the seven energy points in Sol. C. respectively.

a dip structure. The counter-clockwise behavior of the $^3D_1$-amplitude of Sol. A corresponds to the gentle dip structure of $\Delta\sigma_T$ in the range of $T_L = 600 - 700$ MeV in Fig. 3.8. Its resonance parameters are evaluated as $M = 2180$ MeV, $\Gamma = 80$ MeV, elasticity $= 0.04$. Thus its validity can be confirmed by the measurement of $\Delta\sigma_T$ with precision in the energy region.

3.4.6 Experimental data used in this analysis and their references

The following experimental data are used in the present analysis. We use the notation DI(T/N/A), where DI is the data index, T the incident kinetic energy in laboratory system in MeV, N the number of data points, A the angular range in center of mass system in degree. The references corresponding to the data indices are summarized at the end of this subsection. The experimental data with the symbol $*$ in their indices are used only in the SE–PSAs.

T_L = 500 MeV (Total number of data points = 685 (685))

σ_r : BY(87) (500.0 / 1 /), σ_t : NAI(95) (500.0 / 1 /), $\Delta\sigma_T$: NAI(95) (500.0 / 1 /), $\Delta\sigma_L$: NAI(95) (500.0 / 1 /), α : GR(77) (500.0 / 1 /), ReF_2 : GR(78) (500.0 / 1 /), ReF_3 : GR(78) (500.0 / 1 /), $d\sigma/d\Omega$: HU(80) (480.0 / 37 / 140–179), SI(89) (481.0 / 42 / 12–33), KE(82) (493.0 / 6 / 17–97), KE(82) (493.0 / 4 / 57–63), KE(82) (493.0 / 68 / 57–172), BI(75) (494.2 / 43 / 151–180), BO(78) (495.7 / 71 / 117–180), HU(80) (501.0 / 37 / 140–179), BO(78) (518.5 / 75 / 117–180), P : MC(93) (485.0 / 30 / 61–161), MC(95) (485.0 / 18 / 36–109),

CL(80) (495.0 / 19 / 34–161), CL(80) (495.0 / 11 / 68–158), CH(67) (498.0 / 8 / 33–145), MA(86) (500.0 / 3 / 22–44), LE(71) (520.0 / 4 / 90–180), A_{NN} : NAI(95) (500.0 / 14 / 70–122), A_{SL} : DI(92) (484.0 / 20 / 80–175), A_{LL} : DI(92) (484.0 / 21 / 80–178), K_{SS} : MC(92) (485.0 / 5 / 114–176), AM(77) (495.0 / 1 / 160), AX(80) (495.0 / 11 / 65–163), AX(80) (506.4 / 1 / 160), AM(77) (516.0 / 3 / 153–166), LE(70) (520.0 / 4 / 90–180), K_{LS} : MC(92) (485.0 / 7 / 74–176), AX(80) (495.0 / 11 / 65–163), K_{SL} : MC(92) (485.0 / 5 / 114–176), AM(77) (495.0 / 1 / 160), AX(80) (506.4 / 1 / 160), LE(70) (520.0 / 3 / 90–124), K_{LL} : MC(92) (485.0 / 7 / 74–176), K_{NN} : MC(93) (485.0 / 30 / 61–160), CL(80) (495.0 / 17 / 60–158), AM(77) (516.0 / 3 / 153–166), HA(70) (520.0 / 4 / 90–180), D : MA(86) (500.0 / 3 / 22–44), $C_{\sigma\sigma}$: GA(89) (484.0 / 21 / 75–180), R : MA(86) (500.0 / 4 / 22–55), R' : MA(86) (500.0 / 4 / 22–55), A : MA(86) (500.0 / 3 / 22–44), A' : MA(86) (500.0 / 3 / 22–44)

T_L = 530 MeV (Total number of data points = (581))

σ_r : BY(87) (530.0 / 1 /), σ_t : NAI(95) (530.0 / 1 /), $\Delta\sigma_T$: NAI(95) (530.0 / 1 /), $\Delta\sigma_L$: NAI(95) (530.0 / 1 /), α : GR(77) (530.0 / 1 /), ReF_2 : GR(78) (530.0 / 1 /), ReF_3 : GR(78) (530.0 / 1 /), $d\sigma/d\Omega$: BO(78) (518.5 / 75 / 117–180), HU(80) (521.0 / 37 / 140–179), NAI(95) (530.0 / 28 / 10–146), BO(78) (531.6 / 70 / 133–180), SI(89) (532.0 / 41 / 12–31), HU(80) (540.0 / 37 / 140–179), BO(78) (541.6 / 79 / 116–180), P : LE(71) (520.0 / 4 / 90–180), NE(89) (525.0 / 22 / 57–158), BAL(87) (544.0 / 7 / 83–118), BH(81) (565.0 / 15 / 71–166), A_{NN} : NAI(95) (530.0 / 14 / 70–122), BH(80) (565.0 / 15 / 71–166), A_{SL} : NAI(95) (530.0 / 9 / 85–140), A_{LL} : NAI(95) (530.0 / 8 / 80–140), K_{SS} : AM(77) (495.0 / 1 / 160), AX(80) (495.0 / 11 / 65–163), AX(80) (506.4 / 1 / 160), AM(77) (516.0 / 3 / 153–166), LE(70) (520.0 / 4 / 90–180), K_{LS} : AX(80) (495.0 / 11 / 65–163), K_{SL} : AM(77) (495.0 / 1 / 160), AX(80) (506.4 / 1 / 160), LE(70) (520.0 / 3 / 90–124), K_{NN} : CL(80) (495.0 / 17 / 60–158), AM(77) (516.0 / 3 / 153–166), HA(70) (520.0 / 4 / 90–180), D : MA(86) (500.0 / 3 / 22–44), R : MA(86) (500.0 / 4 / 22–55), R' : MA(86) (500.0 / 4 / 22–55), A : MA(86) (500.0 / 3 / 22–44), A' : MA(86) (500.0 / 3 / 22–44)

T_L = 560 MeV (Total number of data points = (470))

σ_r : BY(87) (560.0 / 1 /), σ_t : NAI(95) (560.0 / 1 /), $\Delta\sigma_T$: NAI(95) (560.0 / 1 /), $\Delta\sigma_L$: NAI(95) (560.0 / 1 /), α : GR(77) (560.0 / 1 /), ReF_2 : GR(78) (560.0 / 1 /), ReF_3 : GR(78) (560.0 / 1 /), $d\sigma/d\Omega$: HU(80) (540.0 / 37 / 140–179), BO(78) (541.6 / 79 / 116–180), HU(80) (558.0 / 37 / 139–179), NAI(95) (560.0 / 28 / 10–146), BO(78) (564.9 / 80 / 115–180), BI(75) (570.4 / 69 / 134–180), HU(80) (578.0 / 37 / 139–179), P : BAL(87) (544.0 / 7 / 83–118), NAI(95) (560.0 / 6 / 34–58), BH(81) (565.0 / 15 / 71–166), NE(89) (575.0 / 22 / 57–159), A_{NN} : NAI(95) (560.0 / 14 / 70–122), BH(80) (565.0 / 15 / 71–166), A_{SL} : NAI(95) (560.0 / 9 / 85–140), A_{LL} : NAI(95) (560.0 / 8 / 80–140)

T_L = 580 MeV (Total number of data points = 459 (458))

σ_r : BY(87) (580.0 / 1 /), σ_t : NAI(95) (580.0 / 1 /), $\Delta\sigma_T$: NAI(95) (580.0 / 1 /), $\Delta\sigma_L$: NAI(95) (580.0 / 1 /), α : GR(77) (580.0 / 1 /), ReF_2 : GR(78) (580.0 / 1 /), ReF_3 : GR(78) (580.0 / 1 /), $d\sigma/d\Omega$: BO(78) (564.9 / 80 / 115–180), BI(75) (570.4 / 69 / 134–180), HU(80) (578.0 / 37 / 139–179), KA(56)* (580.0 / 15 / 35–179), NAI(95) (580.0 / 25 / 30–130), SI(89) (582.0 / 42 / 11–30), B0(78) (588.4 / 82 / 114–180), P : BH(81) (565.0 / 15 / 71–166), NE(89) (575.0 / 22 / 57–159), NAI(95) (580.0 / 5 / 22–50), LE(71) (600.0 / 4 / 90–180), A_{NN} : BH(80) (565.0 / 15 / 71–166), NAI(95)** (580.0 / 14 / 70–122), NAI(95)*

(580.0 / 15 / 60–124), A_{SL} : NAI(95) (580.0 / 7 / 60–140), A_{LL} : NAI(95) (580.0 / 12 / 60–140), BAL(88) (630.0 / 12 / 60–115), K_{SS} : LE(70) (600.0 / 4 / 65–180), K_{SL} : LE(70) (600.0 / 3 / 65–102), K_{NN} : HA(70) (600.0 / 5 / 65–180), D : GL(71) (612.0 / 3 / 52–125), R : KA(67) (605.0 / 3 / 70–125), A : BI(71) (605.0 / 4 / 55–125)

T_L = 600 MeV (Total number of data points = (432))

σ_r : BY(87) (600.0 / 1 /), σ_t : NAI(95) (600.0 / 1 /), $\Delta\sigma_T$: NAI(95) (600.0 / 1 /), $\Delta\sigma_L$: NAI(95) (600.0 / 1 /), α : GR(77) (600.0 / 1 /), ReF_2 : GR(78) (600.0 / 1 /), ReF_3 : GR(78) (600.0 / 1 /), $d\sigma/d\Omega$: SI(89) (582.0 / 42 / 11–30), BO(78) (588.4 / 82 / 114–180), NAI(95) (600.0 / 30 / 10–126), BI(75) (609.8 / 70 / 133–180), BO(78) (612.0 / 82 / 114–179), P : NE(89) (575.0 / 22 / 57–159), LE(71) (600.0 / 4 / 90–180), CH(67) (601.0 / 8 / 33–146), KA(67) (605.0 / 3 / 70–125), BI(70) (605.0 / 4 / 55–125), NE(89) (625.0 / 21 / 57–159), A_{NN} : NAI(95) (600.0 / 14 / 70–122), A_{SL} : NAI(95) (600.0 / 9 / 85–140), A_{LL} : BAL(88) (630.0 / 12 / 60–115), K_{SS} : LE(70) (600.0 / 4 / 65–180), K_{SL} : MC(92) (635.0 / 39 / 50–178), K_{NN} : HA(70) (600.0 / 5 / 65–180), D : GL(71) (612.0 / 3 / 52–125), R : KA(67) (605.0 / 3 / 70–125), A : BI(71) (605.0 / 4 / 55–125)

T_L = 630 MeV (Total number of data points = 858 (819))

σ_r : BY(87) (630.0 / 1 /), σ_t : NAI(95) (630.0 / 1 /), $\Delta\sigma_T$: NAI(95) (630.0 / 1 /), $\Delta\sigma_L$: NAI(95) (630.0 / 1 /), α : GR(77) (630.0 / 1 /), ReF_2 : GR(78) (630.0 / 1 /), ReF_3 : GR(78) (630.0 / 1 /), $d\sigma/d\Omega$: BO(78) (612.0 / 82 / 114–179), KA(63)* (630.0 / 21 / 12–180), AM(59)* (630.0 / 16 / 12–180), SI(89) (633.0 / 42 / 11–29), BO(78) (636.2 / 84 / 113–179), EV(82) (647.5 / 146 / 51–180), SH(74)* (649.0 / 32 / 51–178), BI(75) (649.1 / 50 / 146–180), P : NE(89) (625.0 / 21 / 57–159), SI(89) (633.0 / 6 / 12–34), MC(93) (635.0 / 30 / 59–160), DZ(64) (635.0 / 9 / 18–146), ZU(76) (635.0 / 7 / 34–124), GL(93) (643.0 / 21 / 15–94), BAR(89) (647.0 / 8 / 47–118), A_{NN} : NAI(95) (630.0 / 14 / 70–122), A_{SL} : DI(92) (634.0 / 20 / 80–175), A_{LL} : BAL(88) (630.0 / 12 / 60–115), DI(92) (634.0 / 21 / 80–178), K_{SS} : MC(92) (635.0 / 39 / 50–178), K_{LS} : MC(92) (635.0 / 39 / 50–178), K_{SL} : MC(92) (635.0 / 39 / 50–178), K_{LL} : MC(92) (635.0 / 39 / 50–178), K_{NN} : MC(93) (635.0 / 33 / 59–172), D : GL(71) (612.0 / 3 / 52–125), DZ(64) (635.0 / 1 / 112), BAR(89) (647.0 / 8 / 47–118), $C_{\sigma\sigma}$: GA(89) (634.0 / 22 / 75–180), R : BAR(89) (647.0 / 4 / 47–108), R' : BAR(89) (647.0 / 4 / 47–108), A : BAR(89) (647.0 / 4 / 47–108), A' : BAR(89) (647.0 / 4 / 47–108)

T_L = 680 MeV (Total number of data points = (441))

σ_r : BY(87) (680.0 / 1 /), σ_t : NAI(95) (680.0 / 1 /), $\Delta\sigma_T$: NAI(95) (680.0 / 1 /), $\Delta\sigma_L$: NAI(95) (680.0 / 1 /), α : GR(77) (680.0 / 1 /), ReF_2 : GR(78) (680.0 / 1 /), ReF_3 : GR(78) (680.0 / 1 /), $d\sigma/d\Omega$: BO(78) (660.4 / 85 / 112–179), NAI(95) (680.0 / 28 / 10–146), SI(89) (683.0 / 42 / 10–28), BO(78) (684.8 / 84 / 112–179), BI(75) (689.7 / 42 / 149–180), P : GL(93) (643.0 / 21 / 15–94), BAR(89) (647.0 / 8 / 47–118), BH(81) (665.0 / 15 / 72–166), NE(89) (675.0 / 18 / 57–159), CH(67) (702.0 / 8 / 30–143), BAL(87) (719.0 / 10 / 95–128), A_{NN} : BH(80) (665.0 / 15 / 80–166), NAI(95) (680.0 / 14 / 70–122), A_{SL} : NAI(95) (680.0 / 9 / 85–140), A_{LL} : NAI(95) (680.0 / 11 / 60–140), D : BAR(89) (647.0 / 8 / 47–118), R : BAR(89) (647.0 / 4 / 47–108), R' : BAR(89) (647.0 / 4 / 47–108), A : BAR(89) (647.0 / 4 / 47–108), A' : BAR(89) (647.0 / 4 / 47–108)

T_L = 730 MeV (Total number of data points = 581)

σ_r : BY(87) (730.0 / 1 /), σ_t : NAI(95) (730.0 / 1 /), $\Delta\sigma_T$: NAI(95) (730.0 / 1 /), $\Delta\sigma_L$: NAI(95) (730.0 / 1 /), α : GR(77) (730.0 / 1 /), ReF_2 : GR(78) (730.0 / 1 /), ReF_3 : GR(78) (730.0 / 1 /), $d\sigma/d\Omega$: LA(60) (710.0 / 9 / 159–180), NAI(95) (730.0 / 25 / 10–132), BI(75) (730.8 / 62 / 135–180), BO(78) (734.1 / 87 / 111–179), P : BAL(87) (719.0 / 10 / 95–128), NE(89) (725.0 / 18 / 57–159), NAI(95) (730.0 / 7 / 22–50), MA(80) (738.0 / 6 / 46–120), LE(88) (744.0 / 10 / 93–122), A_{NN} : NAI(95) (730.0 / 15 / 60–124), LE(88) (744.0 / 7 / 97–120), A_{SL} : NAI(95) (730.0 / 7 / 84–120), LE(88) (744.0 / 8 / 93–120), A_{LL} : NAI(95) (730.0 / 14 / 60–124)

T_L = 740 MeV (Total number of data points = (799))

σ_r : BY(87) (740.0 / 1 /), σ_t : NAI(95) (740.0 / 1 /), $\Delta\sigma_T$: NAI(95) (740.0 / 1 /), $\Delta\sigma_L$: NAI(95) (740.0 / 1 /), α : GR(77) (740.0 / 1 /), ReF_2 : GR(78) (740.0 / 1 /), ReF_3 : GR(78) (740.0 / 1 /), $d\sigma/d\Omega$: SI(89) (708.0 / 42 / 10–27), LA(60) (710.0 / 9 / 159–180), NAI(95) (730.0 / 25 / 10–132), BI(75) (730.8 / 62 / 135–180), BO(78) (734.1 / 87 / 111–179), BO(78) (770.6 / 98 / 179–110), BI(75) (772.9 / 65 / 135–180), P : 740 CH(67) (702.0 / 8 / 30–143), BAL(87) (719.0 / 10 / 95–128), NE(89) (725.0 / 18 / 57–159), NAI(95) (730.0 / 7 / 22–50), MA(80) (738.0 / 6 / 46–120), LE(88) (744.0 / 10 / 93–122), NE(89) (775.0 / 18 / 58–159), SI(89) (784.0 / 6 / 11–30), RA(82) (790.0 / 6 / 167–178), GL(90) (790.0 / 3 / 9–21), A_{NN} : NAI(95) (740.0 / 14 / 70–122), A_{SL} : NAI(95) (730.0 / 7 / 84–120), LE(88) (744.0 / 8 / 93–120), DI(92) (788.0 / 21 / 75–174), A_{LL} : NAI(95) (730.0 / 14 / 60–124), DI(92) (788.0 / 21 / 75–174), K_{SS} : MC(91) (788.0 / 39 / 47–177), RA(82) (790.0 / 3 / 168–177), K_{LS} : MC(91) (788.0 / 39 / 47–177), K_{SL} : MC(91) (788.0 / 39 / 47–177), RA(82) (790.0 / 3 / 168–177), K_{LL} : MC(91) (788.0 / 39 / 47–177), K_{NN} : MC(93) (788.0 / 33 / 58–171), RA(82) (790.0 / 3 / 168–177), $C_{\sigma\sigma}$: GA(89) (788.0 / 20 / 75–180)

T_L = 800 MeV (Total number of data points = 581)

σ_r : BY(87) (800.0 / 1 /), σ_t : NAI(95) (800.0 / 1 /), $\Delta\sigma_T$: NAI(95) (800.0 / 1 /), $\Delta\sigma_L$: NAI(95) (800.0 / 1 /), α : GR(77) (800.0 / 1 /), ReF_2 : GR(78) (800.0 / 1 /), ReF_3 : GR(78) (800.0 / 1 /), $d\sigma/d\Omega$: SI(89) (784.0 / 42 / 9–26), CA(78) (790.0 / 36 / 10–61), JA(84) (801.9 / 141 / 60–180), BI(75) (814.3 / 65 / 134–180), SH(74) (817.0 / 34 / 50–178), P : SI(89) (784.0 / 6 / 11–30), MC(93) (788.0 / 30 / 57–160), MC(95) (788.0 / 31 / 30–128), RA(82) (790.0 / 6 / 167–178), GL(90) (790.0 / 3 / 9–21), LE(88) (794.0 / 7 / 93–123), GL(93) (797.0 / 21 / 14–94), BAL(93) (800.0 / 10 / 29–62), BAL(93) (800.0 / 29 / 48–122), BY(85) (800.0 / 6 / 33–137), BAR(83) (800.0 / 18 / 14–75), BAR(89) (800.0 / 6 / 58–110), A_{NN} : NA(89) (790.0 / 16 / 48–149), LE(88) (794.0 / 5 / 98–122), BAL(93) (800.0 / 27 / 48–122), BAL(93) (800.0 / 10 / 29–62), A_{SL} : DI(92) (788.0 / 21 / 75–174), LE(88) (794.0 / 8 / 93–121), BAL(94) (800.0 / 28 / 31–147), A_{LL} : DI(92) (788.0 / 21 / 75–174), BI(91) (800.0 / 1 / 178), BAL(94) (800.0 / 26 / 30–141), K_{SS} : MC(91) (788.0 / 39 / 47–177), RA(82) (790.0 / 3 / 168–177), BAL(94) (800.0 / 2 / 48–62), K_{LS} : MC(91) (788.0 / 39 / 47–177), BAL(94) (800.0 / 2 / 48–62), K_{SL} : MC(91) (788.0 / 39 / 47–177), RA(82) (790.0 / 3 / 168–177), K_{LL} : MC(91) (788.0 / 39 / 47–177), K_{NN} : MC(93) (788.0 / 33 / 58–171), RA(82) (790.0 / 3 / 168–177), BAL(94) (800.0 / 2 / 48–64), D : BAR(85) (800.0 / 4 / 14–69), BAR(89) (800.0 / 5 / 58–110), BAL(94) (800.0 / 2 / 48–64), D_{LS} : BAL(94) (800.0 / 2 / 48–62), $C_{\sigma\sigma}$: GA(89) (788.0 / 20 / 75–180), H_{LLN} : BAL(94) (800.0 / 2 / 48–62), H_{SLN} : BAL(94) (800.0 / 2 / 48–62), R : BAR(85) (800.0 / 9 / 14–58), BAR(89) (800.0 / 4 / 69–110), R' : BAR(85) (800.0 / 9 / 14–58), BAR(89) (800.0 / 4 / 69–110), A : BAR(85) (800.0 / 7 / 14–58), BAR(89) (800.0 / 4 / 69–110), A' : BAR(85) (800.0 / 7 / 14–58), BAR(89) (800.0 /

5 / 58–110)

T_L = 830 MeV (Total number of data points = 581)

σ_r : BY(87) (830.0 / 1 /), σ_t : NAI(95) (830.0 / 1 /), $\Delta\sigma_T$: NAI(95) (830.0 / 1 /), $\Delta\sigma_L$: NAI(95) (830.0 / 1 /), α : GR(77) (830.0 / 1 /), ReF_2 : GR(78) (830.0 / 1 /), ReF_3 : GR(78) (830.0 / 1 /), $d\sigma/d\Omega$: CA(78) (790.0 / 36 / 10–61), JA(84) (801.9 / 141 / 60–180), BI(75) (814.3 / 65 / 134–180), SH(74) (817.0 / 34 / 50–178), NAI(95) (830.0 / 25 / 26–132), SI(89) (834.0 / 39 / 10–25), BI(75) (856.8 / 70 / 131–180), P : RA(82) (790.0 / 6 / 167–178), GL(90) (790.0 / 3 / 9–21), LE(88) (794.0 / 7 / 93–123), GL(93) (797.0 / 21 / 14–94), BAL(93) (800.0 / 10 / 29–62), BAL(93) (800.0 / 29 / 48–122), BY(85) (800.0 / 6 / 33–137), BAR(83) (800.0 / 18 / 14–75), BAR(89) (800.0 / 6 / 58–110), RO(70) (830.0 / 5 / 133–167), SI(89) (834.0 / 6 / 11–30), BAL(93) (840.0 / 33 / 48–126), BAL(93) (840.0 / 15 / 49–117), BY(85) (850.0 / 5 / 33–55), BAL(93) (860.0 / 28 / 48–123), BAL(93) (860.0 / 11 / 49–89), A_{NN} : BAL(93) (840.0 / 31 / 48–125), BAL(93) (860.0 / 31 / 48–123), A_{SL} : LE(88) (794.0 / 8 / 93–121), BAL(94) (800.0 / 28 / 31–147), BAL(94) (840.0 / 28 / 50–123), A_{LL} : BI(91) (800.0 / 1 / 178), BAL(94) (800.0 / 26 / 30–141), BAL(94) (840.0 / 30 / 50–126), K_{SS} : RA(82) (790.0 / 3 / 168–177), BAL(94) (800.0 / 2 / 48–62), BAL(94) (840.0 / 3 / 54–74), K_{LS} : BAL(94) (800.0 / 2 / 48–62), BAL(94) (840.0 / 3 / 54–74), K_{SL} : RA(82) (790.0 / 3 / 168–177), K_{NN} : RA(82) (790.0 / 3 / 168–177), BAL(94) (800.0 / 2 / 48–64), BAL(94) (840.0 / 4 / 52–77), BAL(94) (860.0 / 3 / 53–76), D : BAR(85) (800.0 / 4 / 14–69), BAR(89) (800.0 / 5 / 58–110), BAL(94) (800.0 / 2 / 48–64), BAL(94) (840.0 / 4 / 52–77), BAL(94) (860.0 / 3 / 53–76), D_{LS} : BAL(94) (800.0 / 2 / 48–62), BAL(94) (840.0 / 3 / 54–74), H_{LLN} : BAL(94) (800.0 / 2 / 48–62), BAL(94) (840.0 / 3 / 54–74), H_{SLN} : BAL(94) (800.0 / 2 / 48–62), BAL(94) (840.0 / 3 / 54–74)

T_L = 870 MeV (Total number of data points = 581)

σ_r : BY(87) (870.0 / 1 /), σ_t : NAI(95) (870.0 / 1 /), $\Delta\sigma_T$: NAI(95) (870.0 / 1 /), $\Delta\sigma_L$: NAI(95) (870.0 / 1 /), α : GR(77) (870.0 / 1 /), ReF_2 : GR(78) (870.0 / 1 /), ReF_3 : GR(78) (870.0 / 1 /), $d\sigma/d\Omega$: BI(75) (856.8 / 70 / 131–180), NAI(95) (870.0 / 25 / 26–130), SI(89) (884.0 / 43 / 9–24), P : BY(85) (850.0 / 5 / 33–55), BAL(93) (860.0 / 28 / 48–123), BAL(93) (860.0 / 11 / 49–89), NAI(95) (870.0 / 5 / 14–30), BAL(93) (877.0 / 24 / 48–95), BAL(93) (877.0 / 9 / 92–122), BAL(93) (880.0 / 29 / 48–123), BAL(93) (880.0 / 24 / 48–96), BAL(93) (880.0 / 14 / 48–94), BAL(93) (880.0 / 5 / 92–121), BAL(93) (880.0 / 14 / 29–55), BAL(93) (880.0 / 35 / 48–116), A_{NN} : BAL(93) (860.0 / 31 / 48–123), BAL(93) (880.0 / 64 / 29–121), A_{SL} : BAL(94) (880.0 / 37 / 30–148), A_{LL} : BAL(88) (880.0 / 15 / 48–90), BAL(94) (880.0 / 36 / 30–148), K_{SS} : BAL(94) (880.0 / 4 / 50–77), K_{LS} : BAL(94) (880.0 / 4 / 49–77), K_{NN} : BAL(94) (860.0 / 3 / 53–76), BAL(94) (880.0 / 4 / 50–77), D : BAL(94) (860.0 / 3 / 53–76), BAL(94) (880.0 / 4 / 50–77), D_{LS} : BAL(94) (880.0 / 4 / 50–77), H_{LLN} : BAL(94) (880.0 / 4 / 49–77), H_{SLN} : BAL(94) (880.0 / 4 / 50–77)

T_L = 930 MeV (Total number of data points = 581)

σ_r : BY(87) (930.0 / 1 /), σ_t : NAI(95) (930.0 / 1 /), $\Delta\sigma_T$: NAI(95) (930.0 / 1 /), $\Delta\sigma_L$: NAI(95) (930.0 / 1 /), α : GR(77) (930.0 / 1 /), ReF_2 : GR(78) (930.0 / 1 /), ReF_3 : GR(78) (930.0 / 1 /), $d\sigma/d\Omega$: NAI(95) (930.0 / 25 / 26–130), SI(89) (934.0 / 42 / 9–24), BI(75) (941.8 / 70 / 130–180), P : BAL(93) (910.0 / 25 / 48–96), BAL(93) (910.0 / 5 / 97–126), BAL(93) (910.0 / 25 / 48–96), BAL(93) (910.0 / 31 / 48–121), BAL(93) (910.0 / 26 / 48–124), SI(89) (934.0 / 6 / 10–28), BAL(93) (940.0 / 23 / 48–92), BAL(93) (940.0 / 4

/ 98–121), BAL(93) (940.0 / 23 / 48–92), BAL(93) (940.0 / 11 / 49–88), BAL(93) (940.0 / 4 / 98–121), BAL(93) (940.0 / 35 / 29–123), A_{NN} : BAL(93) (910.0 / 19 / 48–121), BAL(93) (940.0 / 41 / 26–122), A_{SL} : BAL(94) (940.0 / 29 / 30–148), A_{LL} : BAL(94) (940.0 / 30 / 30–139), K_{SS} : BAL(94) (940.0 / 4 / 46–71), K_{LS} : BAL(94) (940.0 / 4 / 46–71), K_{NN} : BAL(94) (910.0 / 5 / 52–86), BAL(94) (940.0 / 4 / 48–73), D : BAL(94) (910.0 / 5 / 52–86), BAL(94) (940.0 / 4 / 48–73), D_{LS} : BAL(94) (940.0 / 4 / 46–71), H_{LLN} : BAL(94) (940.0 / 4 / 46–71), H_{SLN} : BAL(94) (940.0 / 4 / 46–71)

T_L = 990 MeV (Total number of data points = 581)

σ_r : BY(87) (990.0 / 1 /), σ_t : NAI(95) (990.0 / 1 /), $\Delta\sigma_T$: NAI(95) (990.0 / 1 /), $\Delta\sigma_L$: NAI(95) (990.0 / 1 /), α : GR(77) (990.0 / 1 /), ReF_2 : GR(78) (990.0 / 1 /), ReF_3 : GR(78) (990.0 / 1 /), $d\sigma/d\Omega$: SI(89) (985.0 / 42 / 8–23), BI(75) (985.3 / 70 / 130–180), NAI(95) (990.0 / 25 / 26–130), MU(67) (991.0 / 16 / 14–150), SH(74) 1(028.0 / 33 / 48–178), P : SI(89) (985.0 / 6 / 10–27), BAL(93) (1000.0 / 42 / 21–150), BAL(93) (1000.0 / 16 / 49–119), MA(78) (1030.0 / 12 / 30–78), A_{NN} : BAL(93) (1000.0 / 40 / 21–150), A_{SL} : BAL(94) (1000.0 / 43 / 30–141), A_{LL} : BAL(88) (980.0 / 8 / 49–83), BAL(94) (1000.0 / 44 / 30–141), K_{SS} : BAL(94) (1000.0 / 4 / 47–77), K_{LS} : BAL(94) (1000.0 / 4 / 47–77), K_{NN} : BAL(94) (1000.0 / 4 / 48–77), D : BAL(94) (1000.0 / 4 / 48–77), D_{LS} : BAL(94) (1000.0 / 4 / 47–77), H_{LLN} : BAL(94) (1000.0 / 4 / 47–77), H_{SLN} : BAL(94) (1000.0 / 4 / 47–77)

T_L = 1090 MeV (Total number of data points = 581)

σ_r : BY(87) (1090.0 / 1 /), σ_t : NAI(95) (1090.0 / 1 /), $\Delta\sigma_T$: NAI(95) (1090.0 / 1 /), $\Delta\sigma_L$: NAI(95) (1090.0 / 1 /), α : GR(77) (1090.0 / 1 /), ReF_2 : GR(78) (1090.0 / 1 /), ReF_3 : GR(78) (1090.0 / 1 /), $d\sigma/d\Omega$: BI(75) (1029.1 / 68 / 131–180), BI(75) (1073.2 / 68 / 130–180), SI(89) (1085.0 / 41 / 9–21), NAI(95)(1090.0 / 22 / 26–130), BI(75) (1117.5 / 68 / 130–180), P : BAL(93) (1080.0 / 10 / 50–86), BAL(93) (1100.0 / 38 / 26–126), BAL(93) (1100.0 / 10 / 50–115), A_{NN} : BAL(93) (1080.0 / 10 / 53–86), BAL(93) (1100.0 / 33 / 26–143), A_{SL} : BAL(94) (1080.0 / 11 / 50–90), BAL(94) (1100.0 / 27 / 26–148), A_{LL} : BAL(88) (1080.0 / 10 / 41–85), BAL(94) (1100.0 / 34 / 29–148), K_{SS} : BAL(94) (1100.0 / 3 / 42–68), K_{LS} : BAL(94) (1100.0 / 3 / 42–68), K_{NN} : BAL(94) (1100.0 / 4 / 43–70), D : BAL(94) (1100.0 / 4 / 43–70), D_{LS} : BAL(94) (1100.0 / 3 / 42–68), H_{LLN} : BAL(94) (1100.0 / 3 / 42–68), H_{SLN} : BAL(94) (1100.0 / 3 / 42–68).

Data references

AM(59) Amaglobeli, N. S., JETP(USSR) **34**(1959)53.
AM(77) Amsler, C. et al., Nucl. Instr. and Method **144**(1977)401.
AX(80) Axen, D. et al., Phys. Rev. **C21**(1980)998.
BAR(83) Barlett, M. L. et al., Phys. Rev. **C27**(1983)682.
BAR(85) Barlett, M. L. et al., Phys. Rev. **C32**(85)239.
BAR(89) Barlett, M. L. et al., Phys. Rev. **C40**(1989)2697.
BAL(87) Ball, J. et al., Nucl. Phys. **B286**(1987)635.
BAL(88) Ball, J. et al., Z.Phys. **C40**(1988)193.
BAL(93) Ball, J. et al., Nucl. Phys. **A559**(1993)477.
BAL(93) Ball, J. et al., Nucl. Phys. **A559**(1993)489.
BAL(93) Ball, J. et al., Nucl. Phys. **A559**(1993)511.
BAL(94) Ball, J. et al., Nucl. Phys. **A574**(1994)697.
BAL(94) Ball, J. et al., Z. Phys. **C61**(1994)579.
BH(80) Bhatia, T. S. et al., 5th International Symposium on Polarization Phenomena in Nuclear Physics, Santa Fe, August 11–15, 1980, Contributed Papers No1.4.
BH(81) Bhatia, T. S. et al., Phys. Rev. **C24**(1981)796.
BI(71) Bilenkaya, S. I. et al., JETP(USSR) **32**(1971)569.
BI(70) Bilenkaya, S.I.et al., Preprint JINR P1–4960, Dubna 1970.
BI(75) Bizard, et al., Nucl. Phys. **B85**(1975)14.
BI(91) Binz, PhD. Thesis, 1991.
BO(78) Bonner, B. E. et al., Bystricky, J. and Lehar, F., Physics Data Nr 11–1, Part I and II(1978) edited by H. Behrens and G. Ebel (Fachinformationszentrum Karlsruhe).
BO(78) Bonner, B. E. et al., Phys. Rev. Lett. **41**(1978)1200.
BY(85) Bystricky, J., Nucl. Phys. **A444**(1985)597.
BY(87) Bystricky, J. et al., J. Physipue **48**(1987)1901.
CA(78) Carlini, R. et al., Phys. Rev. Lett. **41**(1978)1341.
CH(67) Cheng, D. et al., Phys. Rev. **163**(1967)1470.
CL(80) Clough, A. S. et al., Phys. Rev. **C21**(1980)988.
DI(92) Ditzler, W. R. et al., Phys. Rev. **D46**(1992)2792.
DZ(64) Dzhelepov, P. et al., Proceedings of the XIIth International Conference on High Energy Physics, Dubna 1964, Vol. 1, P.11.
EV(82) Evans, M. L. et al., Phys. Rev. **C26**(1982)2525.
GA(89) Garnett, R. et al., Phys. Rev. **D40**(1989)R1708.
GL(71) Glonti, L. N. et al., Preprint JINR P1–5743, Dubna 1971.
GL(90) Glass, G. Phys. Rev. **C41**(1990)2732.
GL(93) Glass, G. Phys. Rev. **C47**(1993)1369.
GR(77) Grain, W., Nucl. Phys. **B131**(1977)255.
GR(78) Grain, W. et al., Nucl. Phys. **B137**(1978)173.
HA(70) Pamela Hansea–Surko, Thises, UCLR–19451, Jan. 15, 1970.
HU(80) Hürster, W. et al., Phys. Lett. **90B**(1980)367.
JA(84) Mahavir Jain, Phys. Rev. **C30**(1984)566.
KA(56) Kazarinov, Yu. M. et al., JETP(USSR) **31**(1956)169.
KA(63) Kazarinov, Yu. M. et al., Preprint JINR P–1207,DUBNA 1963.
KA(67) Kazarinov, Yu. M. et al., Yad. Fiz. **5**(1967)140.

MA(80) Masaike, A., Bystricky, J. and Lehar, F., Physics Data Nr 11–1, Part I and II(1978) edited by H. Behrens and G. Ebel (Fachinformationszentrum Karlsruhe).
MA(86) Marshall, J. A. et al., Phys. Rev. **C34**(1986)1433.
MC(91) McNaughton, M. W. et al., Phys. Rev.**C44**(1991)2267.
MC(92) McNaughton, M. W. et al., Phys. Rev. **C46**(1992)47.
MC(93) McNaughton, M. W. et al., Phys. Rev. **C48**(1993)256.
MC(95) McNaughton, M. W. et al., Preprint LA–UR–95–1358, LAMPF 1995.
MU(67) Murray, T. A. et al., Nuovo Cim. **49**(1967)261.
NA(89) Nath, S. et al., Phys. Rev. **D39**(1989)3520.
NE(89) Newsom, C. R. et al., Phys. Rev. **C39**(1989)965.
RA(82) Ransome, R. D. et al., Phys. Rev. Lett. **48**(1982)781.
RO(70) Rohrish, P. R. et al., Phys. Lett. **31B**(1970)617.
SH(74) Shephard, P. F. et al., Phys. Rev. **D10**(1974)2735.
SI(89) Silverman, B. H. et al., Nucl.Phys. **A499**(1989)763.
ZU(76) Zulkarneev, R. et al., Phys. Lett. **61B**(1976)164.